

# We are IntechOpen, the world's leading publisher of Open Access books Built by scientists, for scientists

6,900

Open access books available

186,000

International authors and editors

200M

Downloads

Our authors are among the

154

Countries delivered to

TOP 1%

most cited scientists

12.2%

Contributors from top 500 universities



WEB OF SCIENCE™

Selection of our books indexed in the Book Citation Index  
in Web of Science™ Core Collection (BKCI)

Interested in publishing with us?  
Contact [book.department@intechopen.com](mailto:book.department@intechopen.com)

Numbers displayed above are based on latest data collected.  
For more information visit [www.intechopen.com](http://www.intechopen.com)



# The Geochemical Data Imaging and Application in Geoscience: Taking the Northern Daxinganling Metallogenic Belt as an Example

*Jiang Chen, Zhaoxia Mao, Yan Zhao, Chunpeng Zhang and Shan Jiang*

## Abstract

Geochemical data were predominantly expressed by vector format, the research on geochemical data visualization, i.e., raster data format, was not paid proper attention. A total of 39 geochemical elements in 1:200,000 regional geochemical exploration data were rasterized to form images, and then a geochemical image database was generated. This article has carried out the study on geochemical imaging within Daxinganling metallogenic belt. The metallogenic belt had once carried out the regional geochemical survey, the sampling density was 1 site/4 km<sup>2</sup>, and 39 geochemistry elements including the microelement and trace element have been analyzed. Quintic polynomial method was used to implement the geochemical data interpolation, and the cell size of formed geochemical elemental image is 1 km. The images of the geochemical elements were processed by image enhancement methods, and then hyperspectral remote sensing data processing method was used for prospecting target selection, lithology mapping, and so on. The interpreted results have been verified in practice. All the abovementioned suggested a good development prospect for the rasterized geochemical images. Finally the author puts forward using rasterize geochemical images in combination with other geological, geophysical, and remote sensing data to make better use of the geochemical data and be more extensively applied in the geoscience.

**Keywords:** rasterization, vector, hyperspectrum, geoscience, geochemical spectral

## 1. Introduction

Geochemical data are typically reported as compositions, in the form of such proportions as weight percents, parts per million, etc., subject to a constant sum (e.g., 100%, 1,000,000 ppm). As an important source of geo-information, geochemical data recording multiple element concentration have been successfully processed by advanced multivariate analytical methods (e.g., factor analysis, cluster analysis, etc.) to identify geological bodies and delineate mineralization-favored space [1–6]. The results of these geochemical data were mainly expressed by vector format, including the colorful geochemical map.

The raster image application in geology was further improved with the development of remote sensing technology. With respect to the application of remote sensing in geology, several books on the geological structural interpretation were published [7, 8]. As the multispectral and hyperspectral imaging rapidly grows, most of the researches paid much attention to the extraction of altered mineral information which were often related to different types of ore deposits [9–16]. These ore deposits include Carlin-type deposit, Archean massive sulfide deposit, skarn-type deposit, and volcanic massive sulfide deposit. Some studies also focused on lithology mapping with hyperspectral tools [17–22].

Only little geochemical data was rasterized. It is partly because the rastering process is more complex, and also the formed raster image could not produce good visual effect due to the low sample density. It is worth mentioning that the geochemical data with vector format can provide relatively simple results; thus the rasterized image appears superfluous. A small amount of research focused on geochemical data rasterization. A technique of metal content on maps was developed [23]. Utilizing ALKEMIA software, Gustavsson et al. [24] designed an interpolation and smoothing method to generate maps including dot maps, color maps, and shaded relief maps.

In this study, geochemical data of the northern Daxinganling metallogenic belt were taken as the experiment area.

A geochemical survey with the scale of 1:200,000 was conducted in a large area of the Daxinganling region [6]. In follow-up to that research, the objectives of the present study are to evaluate the rasterization method of geochemical data obtained from the northern Daxinganling region, use rasterized geochemical data to assist in geological mapping and prospecting target selection, and propose an application of rasterized geochemical data.

## **2. Experimental area and method**

### **2.1 Experimental area**

The northern Daxinganling metallogenic belt was chosen as an experimental area. The Daxinganling metallogenic belt generally refers to an area including the main ridge of the Daxinganling Mountains and both of its east and west slopes.

### **2.2 Geological background**

The Daxinganling region generally refers to an area that includes the main ridge of the Daxinganling Mountains and the eastern and western slopes of the ridge (**Figure 1**). The region is located between the Siberian and North China plates [26, 27]. Several of its tectonic units had been divided (**Figure 1**). In this region, the Proterozoic strata are comprised of epicontinental detritus from volcanic eruptions and carbonate sedimentary formations. The strata constitute the Precambrian crystalline basement [26]. The cap rock is composed of the Paleozoic group, including the Ordovician, Silurian, Devonian, and Carboniferous series, which are sets of epicontinental clastic rock, specifically carbonate rocks interlayered with rock from volcanic eruptions and sedimentary formations. The Mesozoic, Jurassic, and Cretaceous series are primarily comprised of rock from nonmarine volcanic eruptions and sedimentary formations. An important area of concentrated mineralization exists in the western region of the Hulunhu-Eerguna fault (fault ① in **Figure 1**). In this area, many deposits exist [28]. The mineralization is mainly subvolcanic-hydrothermal-type deposit and porphyry deposit. The porphyry deposit is predominantly comprised

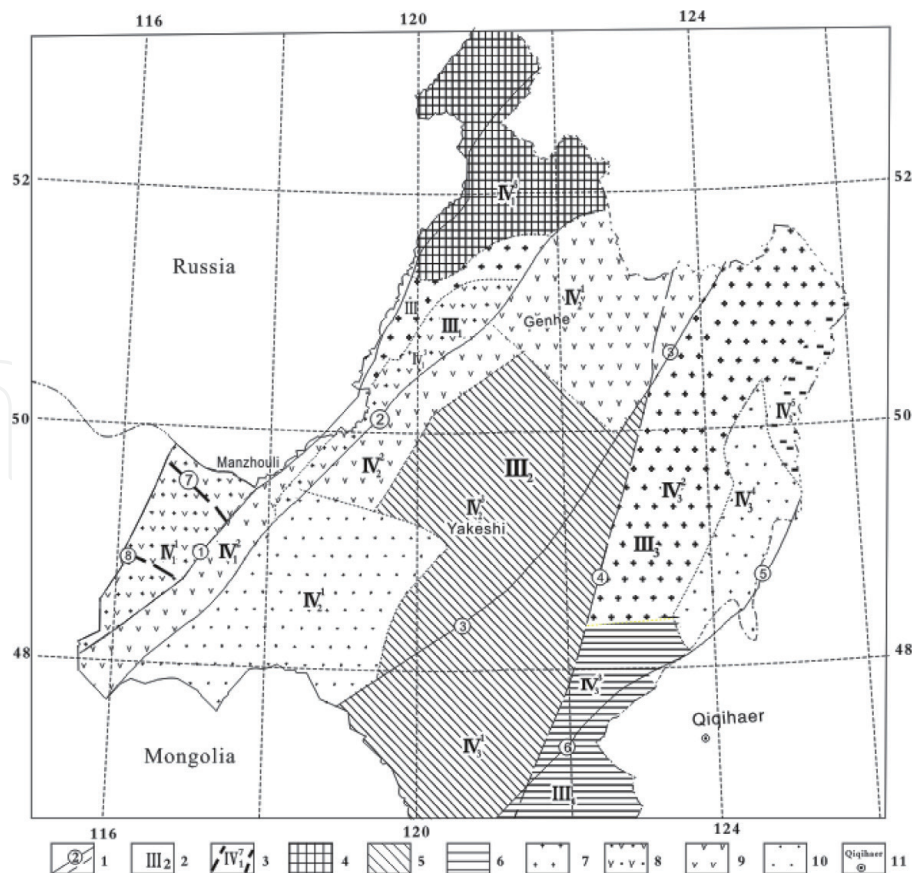


**Figure 1.** Geotectonic units of northern Daxinganling metallogenic belt (after [25]). 1, main fault and borderline of the third-order geotectonic unit; 2, the number of third-order geotectonic unit; 3, the number of fourth-order geotectonic unit; 4, Proterozoic lift; 5, early Paleozoic lift; 6, late Paleozoic lift; 7, magmatic area mainly activated in Hercynian period; 8, lift of Mesozoic volcanic and intrusive rocks; 9, basin of Mesozoic volcanic rocks; 10, Cretaceous fault-depression basin; 11, town. The name of main fault: ①, Hulunhu-Eerguna fault; ②, De'erbugan fault; ③, Elunchun-Toudaoqiao fault; ④, Daxinganling main ridge fault; ⑤, Nenjiang fault; ⑥, Arongqi fault; ⑦, Muhaer fault; ⑧, Haligou fault.

of substantial deposits of Wunugetushan porphyry copper, as well as Jiawula and Chaganbulagen lead, zinc, and silver [25].

### 2.3 Geochemical data

The northern Daxinganling metallogenic belt has two major geographic landscapes, i.e., forest swamp area and semidesert area. The sampling media differed in the two landscapes [29]. The northern Daxinganling metallogenic belt has two major geographic landscapes, i.e., forest swamp area and semidesert area. The sampling media differed in the two landscapes [29]. The 1:200,000 geochemical survey was completed in the Manzhouli area, which covers a total of 13 geological sheets (e.g., Toudaolvodian (M-50-(24)), Manzhoulishi (M-50-(22)), etc.). The geochemical survey was based on stream sediment [30]. The average sampling density was one site per 4 km<sup>2</sup>. Sampled material was passed through a 40-mesh sieve before being sent for analysis in the laboratory [31]. The contents of a total of 39 elements, of which seven were major elements, were analyzed, specifically Al, Ca, Fe, K, Mg, Na, Si, and the 32 trace elements (Ag, As, Au, B, Be, Ba, Bi, Cd, Co, Cr, Cu, F, Hg, La, Li, Mn, Mo, Nb, Ni, P, Pb, Sb, Sn, Sr, Th, Ti, U, V, W, Y, Zn, and Zr) [29]. Because 39 kinds of elements are painstakingly picked out, many elements are quite representative. From the periodic table of the elements shown in **Figure 2**, it can be seen that every family has at least one representative element except family 16 and 18.

## 2.4 Geochemical data rasterizing method

The remote sensing software can be used for the point rastering; most of the data processing and interpretation can be accomplished. In this study, the whole process was completed through using the ENVI software (V. 4.4, Research System Inc., Boulder, CO, USA).

### 2.4.1 Conversion of data format

The geochemical data obtained from the Daxinganling Mountains were stored in Microsoft XLS format, and 39 elements (oxide) data was included. The arrangement of single elements' data is based on the seriation of the first letters and then followed by oxide. The whole arrangement order is as follows: Ag, As, Au, B, Ba, Be, Bi, Cd, Co, Cr, Cu, F, Hg, La, Li, Mn, Mo, Nb, Ni, P, Pb, Sb, Sn, Sr, Th, Ti, U, V, W, Y, Zn, Zr, Al<sub>2</sub>O<sub>3</sub>, CaO, Fe<sub>2</sub>O<sub>3</sub>, K<sub>2</sub>O, MgO, Na<sub>2</sub>O, and SiO<sub>2</sub>. The oxides content were expressed in percentage; the unit of Au and Ag value is ppb. The units of other content values all were ppm. The geographic position was expressed in the format of geographic coordinates.

The file needs to be checked in the sorting way, to inspect whether unqualified data exists. The unqualified data site must be eliminated to ensure quality of the data. Because ENVI cannot directly recognize the file with Microsoft XLS format, the XLS files need to be transformed into TXT format. The latitude and longitude of coordinates were assigned at the first two columns respectively; the other elements were listed afterwards. In Microsoft Excel, the file was saved as TXT format. Additionally, it needs to be noted that if the data content of the geochemical exploration sampling sites is too large even exceeding the permission of Microsoft Excel software, then respectively they need to be else saved in other software, e.g., software Surfer 8 (Golden Software Inc., Golden, USA), to obtain the format that can be recognized by ENVI software. The latter case is suitable for the aeromagnetic data, in which data volume is enormous and usually exceeds the row range of Microsoft Excel software.

### 2.4.2 Rasterizing geochemical data

The geochemical data are rasterized by pull-down menu "Rasterize point data" in the ENVI software. The output projection was determined, and output X/Y size was selected as 1000 m, meaning the spatial resolution of the formed rasterized images is 1000 m. Linear interpolation (quintic polynomial) was chosen. Smooth quintic

1																2		
H																He		
3	4											5	6	7	8	9	10	
Li	Be											B	C	N	O	F	Ne	
11	12											13	14	15	16	17	18	
Na	Mg											Al	Si	P	S	Cl	Ar	
19	20	21	22	23	24	25	26	27	28	29	30	31	32	33	34	35	36	
K	Ca	Sc	Ti	V	Cr	Mn	Fe	Co	Ni	Cu	Zn	Ga	Ge	As	Se	Br	Kr	
37	38	39	40	41	42	43	44	45	46	47	48	49	50	51	52	53	54	
Rb	Sr	Y	Zr	Nb	Mo	Tc	Ru	Rh	Pd	Ag	Cd	In	Sn	Sb	Te	I	Xe	
55	56	57-70	71	72	73	74	75	76	77	78	79	80	81	82	83	84	85	86
Cs	Ba	*	Lu	Hf	Ta	W	Re	Os	Ir	Pt	Au	Hg	Tl	Pb	Bi	Po	At	Rn
87	88	89-102	103	104	105	106	107	108	109	110	111	112	114					
Fr	Ra	**	Lr	Rf	Db	Sg	Bh	Hs	Mt	Uun	Uuu	Uub	Uuq					
		*Lanthanide series	57	58	59	60	61	62	63	64	65	66	67	68	69	70		
			La	Ce	Pr	Nd	Pm	Sm	Eu	Gd	Tb	Dy	Ho	Er	Tm	Yb		
		**Actinide series	89	90	91	92	93	94	95	96	97	98	99	100	101	102		
			Ac	Th	Pa	U	Np	Pu	Am	Cm	Bk	Cf	Es	Fm	Md	No		

Figure 2.

Position of the elements measured by 1:2,000,000 regional geochemical survey in the periodic table, with shaded area as measured elements.

polynomial interpolation is performed by giving binary interpolation of Z values and smooth surface fitting at points that are irregularly distributed on the X-Y plane. The interpolation function is a fifth-degree polynomial in X and Y in a triangular cell and each polynomial is determined by the given values of Z and estimated values of partial derivatives at the vertexes of the triangle [32]. After the above steps, the image of a single element can be formed. And in the same way, the images of 39 elements can be created.

The sampling sites were irregular and the rasterized image covered a whole area in a rectangle in the process of rasterizing geochemical data (**Figure 3**). These inappropriate image contents can be eliminated by using the method of masking. To mask the incorrect area, the buffer zones of sampling site were used.

The formation of the buffer zone is that the geochemical sampling sites were overlaid by the ROI (region of interest) sites. The overlaid 5231 sampling sites were shown in **Figure 4**. By contrast, the maximum distance assigned to 2 pixels is much better to generate buffer zone. Buffer zone image was used to create an image mask. Finally the incorrect area was masked to generate the geochemical content image (**Figure 5**).

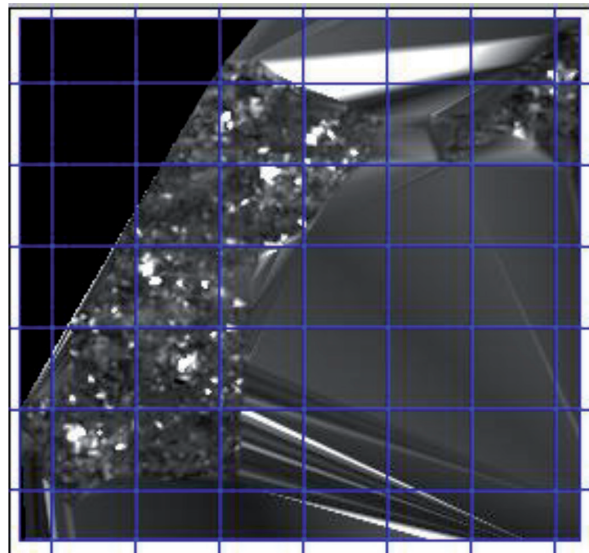


**Figure 3.** Original Ag element grid map of Manzhouli area cut from northern Daxinganling metallogenic belt. Pixel size is 1000 m.

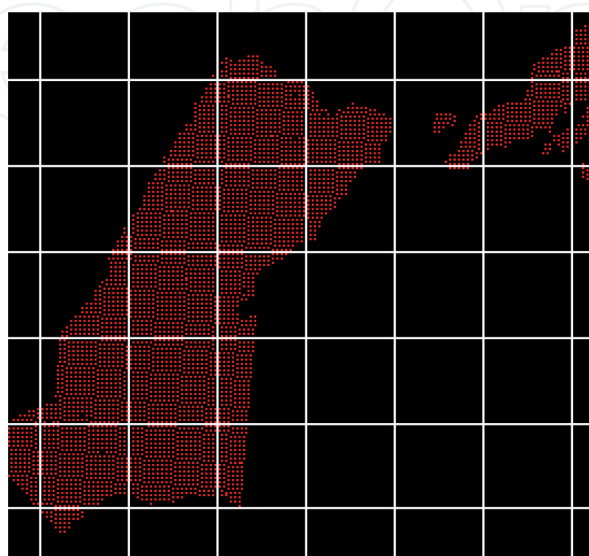


**Figure 4.** Locations of sampling points in Manzhouli area. Sampling points were expressed in ROI and superposed on image maps as pixels. Pixel size is 1000 m.

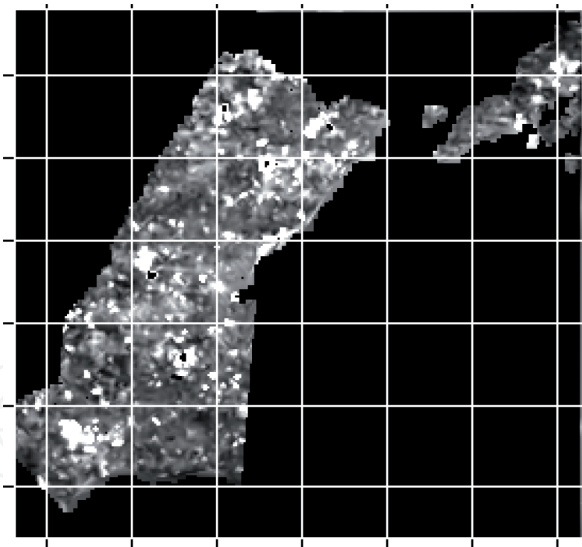


**Figure 5.**  
*Rasterized image of Ag element after a buffer zone mask.*

### 3. Results

#### 3.1 Building geochemical atlas

After 39 kinds of geochemical elements (or oxide) were generated, they would be put together to form an image atlas. The method is simple, namely, using “Laystacking” command, respectively, each image was successively overlaid together.

From the view of spectroscopy, the geochemical elements need to be classified. In the periodic table of the elements, elements of the same family possess similar chemical properties, and they have similar enrichment characteristics in the earth. In accordance with the periodic table, the element family was arranged from left to right. In each family, the order was arranged from top to bottom. In this way, the order of the arranged geochemical elements was as follows: Li, Na<sub>2</sub>O, K<sub>2</sub>O, Be, MgO, CaO, Sr, Ba, Y, La, Th, U, Ti, Zr, V, Nb, Cr, Mo, W, Mn, Fe<sub>2</sub>O<sub>3</sub>, Co, Ni, Cu, Ag, Au, Zn, Cd, Hg, B, Al<sub>2</sub>O<sub>3</sub>, SiO<sub>2</sub>, Sn, Pb, P, As, Sb, Bi, and F.

#### 3.2 Geochemical spectrum

In ENVI software, it is very easy to form the spectra which are constituted of the results of different geochemical elements. This paper defined these spectra as geochemical spectra, which is somewhat similar to the geochemical anomaly and the geochemical chart mentioned in geochemistry, all of which imply the content of geochemical element. All the data in the element content image are with original value, which is easy for data comparisons. If only considering the characteristic of the spectrum, methods of normalization may be adopted, namely, histogram stretching was conducted on each element content image to form the numerical range from 0 to 1, thus creating a clearer and more obvious contrast geochemical spectrum. **Figure 6** shows a comparison of the spectrum of main ore deposits in the Manzhouli region. The ore deposits shown in **Figure 6** are Sanhe lead-zinc deposit, Xiahulin lead-zinc deposit, Waixinhe molybdenum deposit, Babayi copper deposit, Wunugetushan copper-molybdenum deposit, Jiawula lead-zinc deposit, Chaganbulagen lead-zinc-silver deposit, and Erentaolegai silver deposit, respectively.

### 3.3 Image display and image enhancement

The rasterized geochemical image (Figure 7) may be carried out by image enhancement. For example, if expanding or changing the value field range of gray scale, or changing the distributional pattern of gray value, the sharpness of image may be enhanced. Some methods, e.g., direct gray transformation, histogram equalization, etc. may be adopted. And in order to make the edge of the image bright and clear, the image filtering method could be used. The image formed from geochemical data can constitute the ternary RGB image, e.g., the formed  $K_2O-Na_2O-SiO_2$  image (Figure 8); it is known that K-Na-Si ingredient can be used to judge the composition of rocks.

### 3.4 Image statistics

Geochemical image can carry out a numerical statistics, which are somewhat different from the statistics of data of geochemical sampling sites. It is statistics of

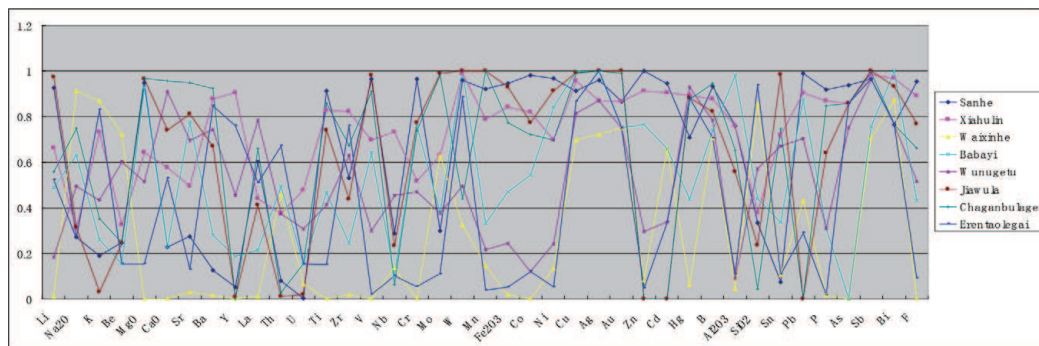


**Figure 6.**  
 Geochemical spectrum of typical deposits in Manzhouli region after histogram stretching.

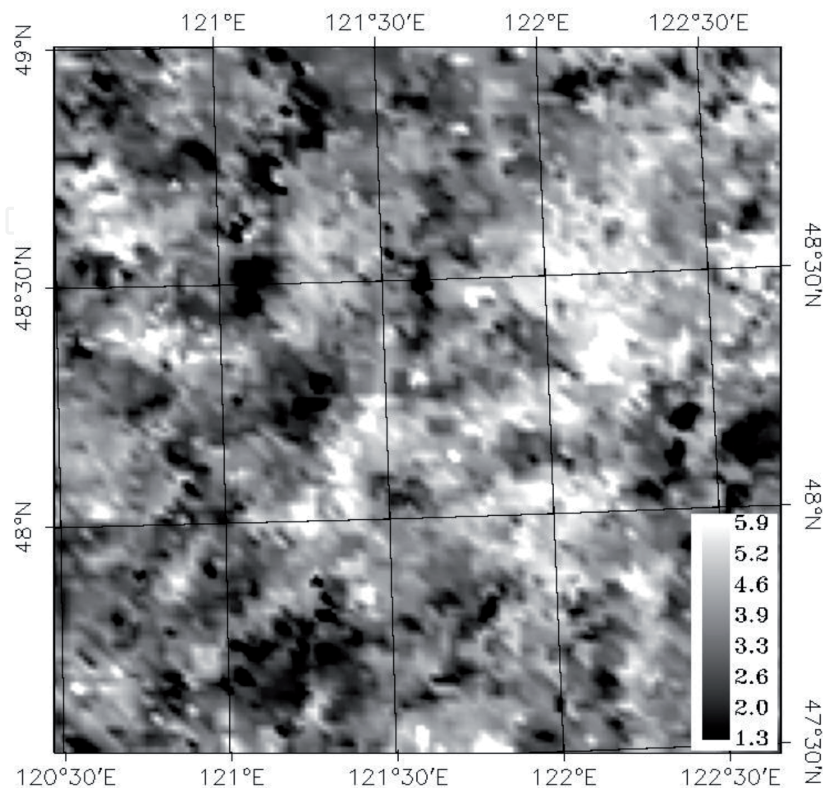


**Figure 7.**  
 Rasterized grayscale map of  $Na_2O$  element content in the middle segment of Daxinganling metallogenic belt.

all the pixels within the image. Basic statistics of a geochemical image involves the mean value, median, mode, range, contrast, etc.

Histogram is one of the important statistics of a geochemical image. Histogram refers to a discrete graph of probability density function of all gray values in the image, or it may be seen as a graphic expression of basic statistics of gray image.

**Figure 9** is based on histogram and the chiefly related statistics. Under ENVI software, the calculation results of cumulative frequency can be obtained, and classification based on histogram analysis will be introduced in the next step.

Density slices to a gray geochemical image can create element anomalies. Cumulative frequency percentage can be used to determine anomalies or anomalies grading (**Figure 10**).

### 3.5 Algebraic operations and logic operations of image

Algebraic operations of image indicate that the corresponding image pixels of two (or more than two) of input images received four arithmetic operations, which in order are addition, subtraction, multiplication, and division. The algebraic operation cannot be directly fulfilled within the vector maps, while the rasterized maps can be directly performed.

Logical operations of images are widely applied, for instance, the masking method mentioned above used logic operations to form a mask band. A specific value in a pixel could be obtained by logical operations, and then a simple classification could be generated.

### 3.6 Geochemical image classification

In the vector image, undoubtedly, the anomaly image of elements is one of the final products in geochemistry. The anomaly map of elements may give users vivid

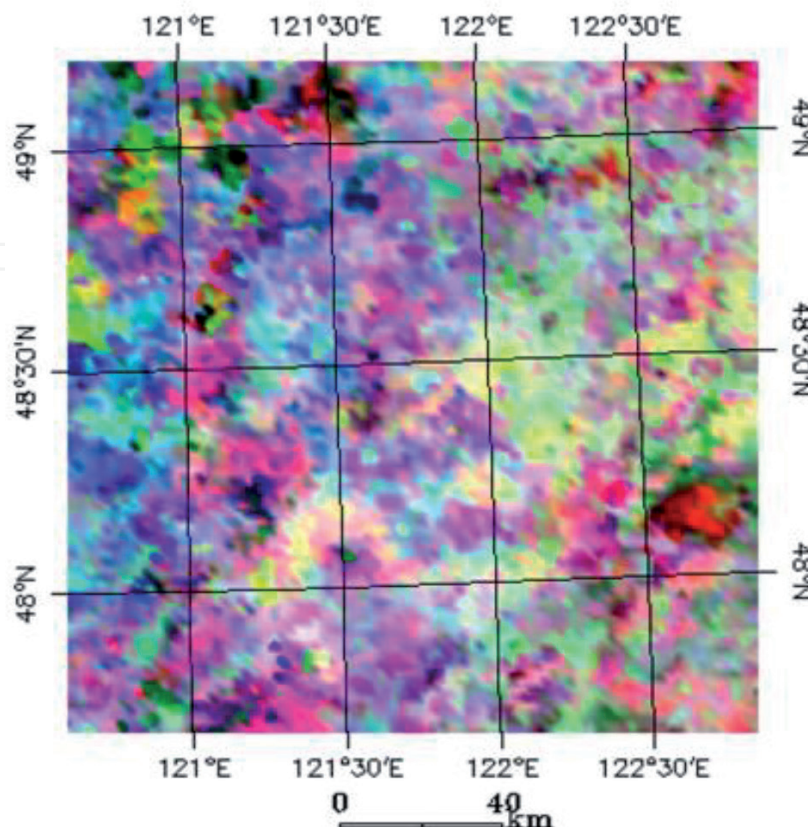


**Figure 8.**  $K_2O$ ,  $Na_2O$ , and  $SiO_2$  ternary color image synthesis in the middle segment of Daxinganling metallogenic belt.

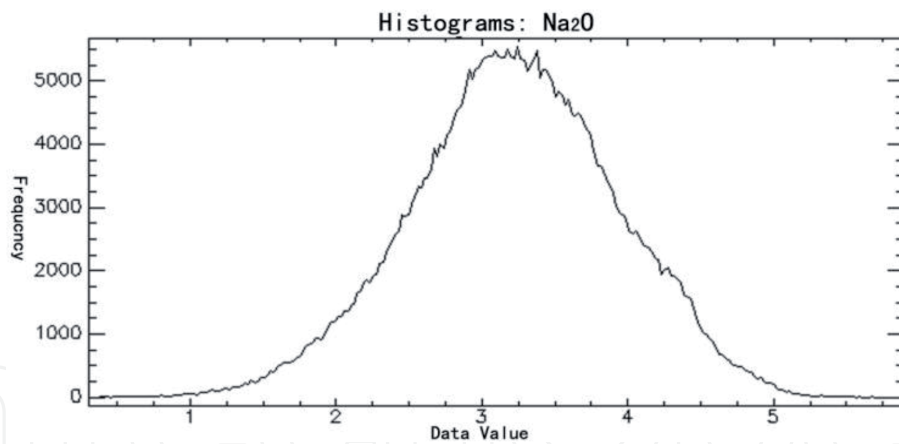


**Figure 9.**  
*Numerical statistical histogram of Na<sub>2</sub>O content in the middle segment of the Daxinganling metallogenic belt.*

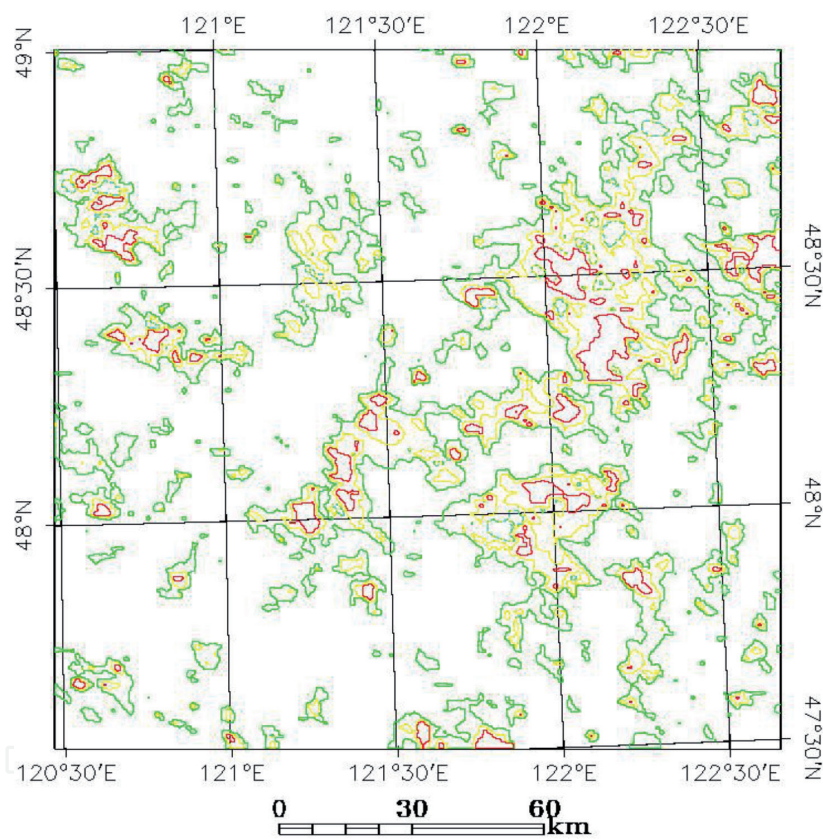


**Figure 10.**  
*Anomaly map of copper element formed in density slice in the middle of the Daxinganling metallogenic belt. According to histogram cumulative frequency statistics, anomalies were graded to 75% (green line), 85% (yellow line), and 95% (red line).*

visual impression. Thus prospecting researchers can directly use the geochemical anomaly maps to explore the interested target. The results expressed in the rasterized image can also be fully used so as to employ the statistical method of density slicing. **Figure 10** is a density sliced map which was created by histogram statistics of copper element, and its result is similar to the geochemical anomaly map. Their difference is that the final rasterized image was irregularly dentate if enlarging a small area.

What is mentioned above is the simplest classification in the rasterized geochemical image, and they were based on the sole element anomaly. Most of the time, the classification using remote sensing images is divided by supervised one and unsupervised one, and their difference is that the supervised classification

firstly gives category, whereas the unsupervised one is determined by the statistics characteristics of image data itself. The classification method used for remote images are suitable for the geochemical atlas. Usually employed methods include multilevel slice classifier, decision tree classifier, minimum distance classifier, maximum likelihood classifier, and the like (e.g., method of fuzzy theory, expert system method, etc.). SAM method mentioned later is one of the supervised classification methods.

## **4. Application of geochemical image in geology**

The formed geochemical atlas can provide the prospecting target area just like conventional geochemical method and may also conduct multielement geochemical analysis. The geochemical image can accomplish the structural interpretation, e.g., linear structure and ring structure in geology just like what is fulfilled by the optical remote sensing. This paper does not restate these traditional methods but will mainly introduce the following three kinds of application in geology in the northern Daxinganling metallogenic belt.

### **4.1 Assisting in geological mapping**

The geochemical atlas of 39 geochemical elements was generated in the northern Daxinganling metallogenic belt, including major elements and trace elements. The full use of all the elements will better assist geological mapping. Especially, in the Daxinganling Mountains, the outcrop is scarce because of the forest cover and that the field work of geological mapping encounters a great deal of difficulties. Therefore, boundaries of the geological bodies are indistinct, and the final boundaries are somehow judged by subjective experience. To employ unsupervised classification method may provide the reference for determining the boundaries of rock in the working area. As shown in **Figure 11**, the Chaihe area in the northern Daxinganling metallogenic belt was taken as an example; this working area belongs to stream sediment survey of the 1:200,000 Wuchagou sheet. The 39 geochemical element images are classified by K-Mean classification, and the geological interpretation map is created as the following one.

It can be seen that the geochemical mapping (**Figure 12**) may relatively clearly distinguish  $\gamma_5^{2(2)}$  alkali feldspar granite from monzogranite. However, the boundary is different from that in the geological map (**Figure 11**). In the north and south, it was verified; but in the east of the map sheet, the rock which was delineated by geochemical images (**Figure 12**) was not presented in the geological map (**Figure 11**). Other Wuchagou basalt can also be easy to identify; two signs were manifested in the north, same as the geological map. Because Baoshi formation and Fujiawazi formation are volcanic, it is sometimes difficult to classify them. As a result, the interpenetration phenomenon is frequent. In the field work, it is hard to distinguish the volcanic rocks. For example, both Fujiawazi formation and Baoshi formation contain tuff; sometimes, the difference between intermediate lava and acidic lava is weak in the field. In this case, the divided geological map is worse than the geochemical classification.

### **4.2 Prospecting target selection**

There is plenty of research on the methods of the prospecting target selecting using data-driven and knowledge-driven modes. In the past, selecting prospecting area was primarily based on the anomaly of the major ore-forming elements. The area with high anomaly value of a single element or integrated anomalies was selected

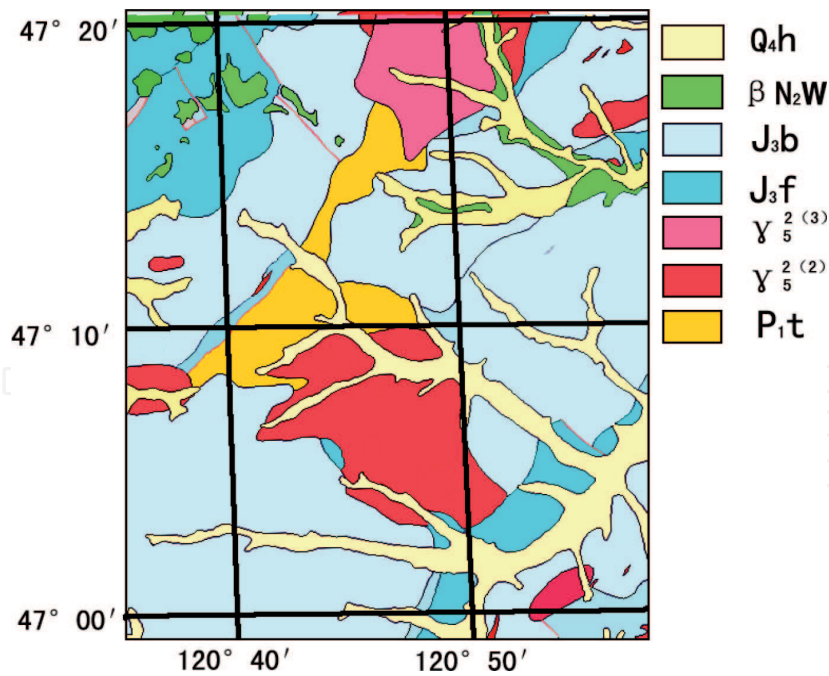


**Figure 11.**  
 Geological sketch of Chaihe area (1:200,000).

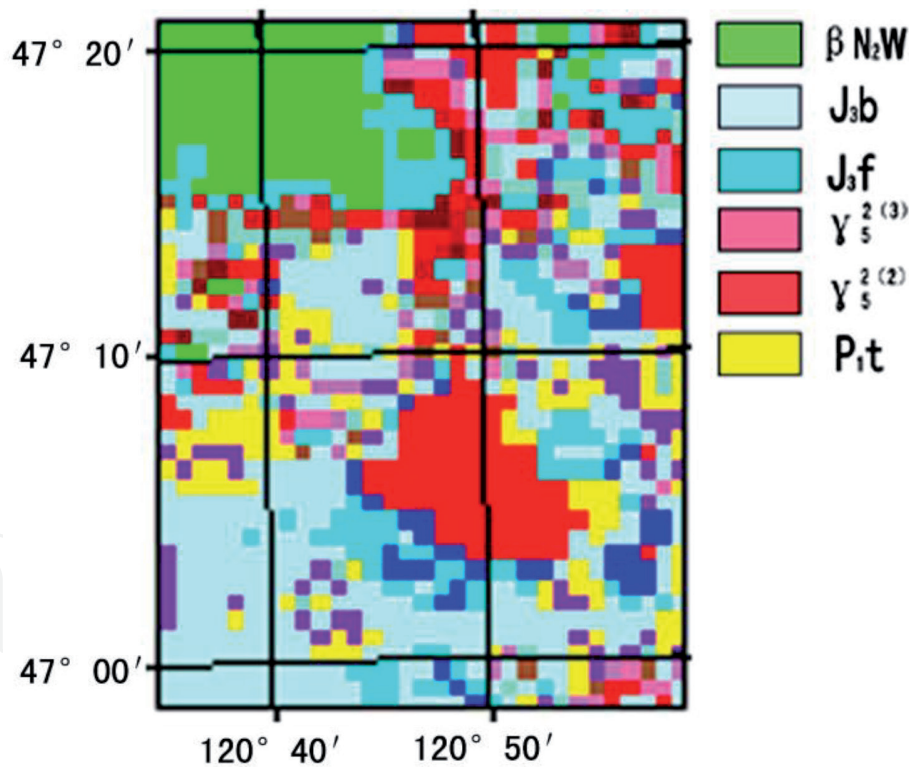


**Figure 12.**  
 Map of each unit of K-Mean classification of 39 geochemical elements in Chaihe area (legend codes are the same as Figure 12).

as prospecting target. Although the large area of geochemical working had been carried out, fewer researchers utilize all elements for prospecting target selecting.

Combining the characteristics of the geochemical atlas in the northern Daxinganling metallogenic belt, the geochemical spectrum method may be adopted to exhibit the similarity with the known deposits on target locating. The most frequently used method is spectral angle mapper method (SAM) [33, 34]. SAM method utilize N-dimensions angle to match image elements and reference

spectra. The geochemical spectra were regarded as vector, whose number of dimensions is the same as the number of waveband. Then using the angle algorithm for calculating the angles' inter-element geochemical spectra, the similarity of two geochemical spectra could be determined. The geochemical spectra of

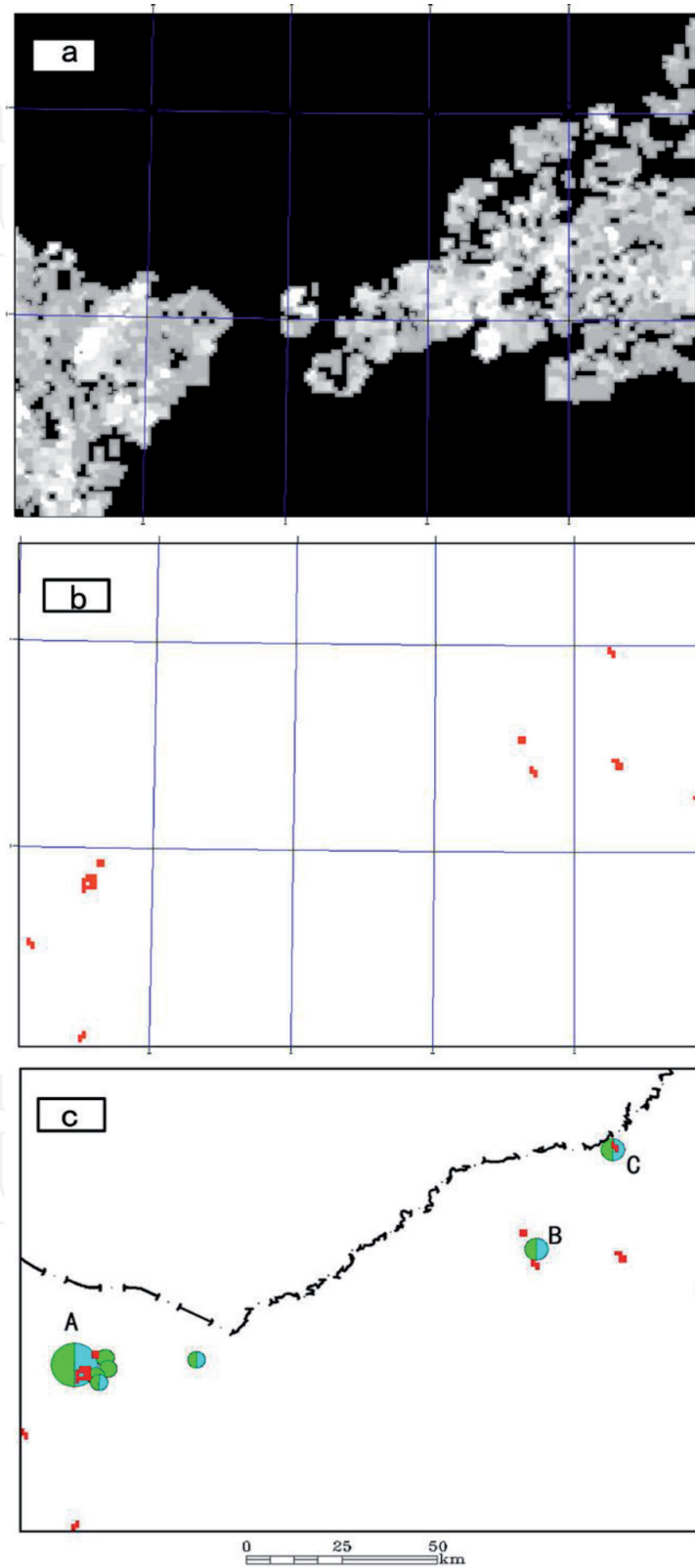


**Figure 13.** Comparison map between the prospecting target and actual deposits in the Manzhouli region. The prospecting target was obtained by applying spectra angle method to some porphyry copper-molybdenum deposit; a is spectral angle map; b is the prospecting target formed by threshold segmentation of spectral angle map; and c is the corresponding location map between prospecting target and actual deposit. A is Wunugetushan deposit, B is Babayi deposit, and C is Badaguan deposit.

locations on the known deposits are regarded as end-member spectra, and then SAM is used to compare end-member spectra with the angles of each pixel vector in N-dimensions space. The smaller angle indicates that it fits better with the geochemical spectra of the discovered deposits. This method fully utilized the information of geochemical spectra and makes every elements involved in the classification. Additionally it emphasizes the shape characteristics of the geochemical content and greatly reduces the information such as the main ore-forming elements.

In this study, the geochemical spectral of the Wunugetushan copper deposit was taken as reference spectra, the SAM method was adopted, and the classification results have been verified by deposits of the same type (**Figure 13**).

#### **4.3 The classification on mixed rocks**

Since the late 1950s, Webb and his colleagues presented to collect fine granular sedimentary from drainages which stands for the average content of the catchment basins [35]. The subsequent regional geochemistry survey mainly based on their theory and method, namely, the sample collected, may stand for the contribution of all matters in the surrounding area of this sampling position. This is the same as to the so-called mixed spectra in remote sensing. Because large areal distributional mixed pixels evidently affect the calculation and classification of the remote sensing image, many researchers put forward the method of decomposing mixed pixels. Nowadays, methods of decomposition of mixed pixels are mainly classified into two classes, one is the linear spectral decomposition, which is based on the linear additivity of brightness of pixels, and the other is the fuzzy decomposition method.

In the process of geological mapping, the stratigraphic unit needs to be divided, and it includes various kinds of rocks. The Manitu formation on the Xiaodonggou section in the northern Daxinganling metallogenic belt served as an example. The standard strata, which were distributed between upper Baiyingaolao formation and lower Manketouebo formation, are 690.6 m thick. From bottom to top, the section involves green andesite (101.6 m), light gray andesitic-rhyolitic breccia tuff (219 m), dark gray, yellow gray andesite interlayered with debris tuff (190.3 m), and purple gray-dark andesite (179.7 m). In the fieldwork, it is difficult to observe all the rock types mentioned due to a few outcrops. As a result, the stratigraphic division can only be based on the limited artificial outcrops. Under this condition, the method of decomposing mixed pixels was used. Through decomposing the mixed pixels, the shares of various kinds of rocks can be achieved; thus it can assist stratigraphic unit classification in geological mapping.

### **5. Discuss and future prospects**

In the past, regional geochemistry has made significant achievements in geology and mineral exploration. However, all of these relied on vector data, and the number of geochemical elements is limited, which narrowed the application of geochemical data. This paper only aims to supplement and modify the shortcomings of previous methods, rather than to overthrow or criticize the achievements attained by them.

The rasterized geochemical image possesses many advantages. The geochemical image is vivid for the visual interpretation. Additionally, data can be compatible for statistical analysis. That vectorized geochemical data accomplished can be achieved by the rasterized data in most cases. Furthermore, the imaged geochemical data could be processed with hyperspectral tools, which cannot be used in vector data.

The shortcoming of rasterized geochemical images mainly lies in that the raster format occupy a relative larger data storage space, and if the sampling sites is sparse, and the spatial resolution is set largely, a clear lattice shape will be displayed.

The increased geochemical density makes this kind of method to get more in-depth application. No doubt geochemical survey with larger scale can provide more information. China recently carries out geological survey on main metallogenic belts, and their sampling density was bigger. The sampling density in the northern Daxinganling metallogenic belt was averagely 4–8 sites per km<sup>2</sup> in the scale of 1:50,000; therefore the sampling density has been greatly increased. Followed by reducing the analysis data of geochemical elements, the usual analyzed elements now are Au, Ag, Cu, Pb, Zn, As, Sb, Hg, W, Sn, Bi, Mo, and so on; the purpose is for mineral exploration. With the increase of sampling data in unit area, the spatial resolutions of geochemical image will increase. The following job is to merge 39 geochemical elements of 1:200,000 with geochemical elements in 1:50,000 to create the multielement geochemical atlas with a relative higher resolution.

Integration with other types of geoscience data is also imperative. The geological map can finally transform to a rasterized image. The strata, magmatism, and so forth may be assigned values through various kinds of logical operations in rasterized image. Regional geophysical survey, for instance, aeromagnetic, airborne gravity, geomagnetic, gravity, and regional electrical method, may form the corresponding rasterized image. These data combined with the geochemical data will undoubtedly increase the information content of geosciences; therefore, it will develop a broader approach for intensive geological study and the comprehensive application of geosciences data.

## **6. Conclusions**

Regional geochemical data of 1:200,000 in the northern Daxinganling area were rasterized using a method that triangulates a planar set of points. Consequently, a multilayered image database containing 39 elements/oxides was formed. The images were enhanced using an image enhancement technique and algebraic operations. The images were handled as multidimensional vector data. Accordingly, hyperspectral tools could be used for the processing. The geochemical signatures of deposits were extracted from the images. Enriched and depleted elements were distinguished by comparing them with regional geochemical statistics. The geochemical signatures represented the geochemical characteristics of ore deposits. The rock types were classified using the K-Means method, which assisted in the regional geological mapping, especially in the areas of dense forest. The geochemical signature of a typical ore deposit was processed by SAM, which determined the similarity between the deposit and pixels in the region. The prospecting target area was determined according to the angle. With increased geochemical data sampling density, as well as further integration with other geophysical, geological, and remote sensing data, rasterized geochemical images can be fully used in the future.

## **Acknowledgements**

This research was supported by funds from the Chinese Ministry of Science and Technology (grant no. 2016YFC0600103) and the “Comprehensive integration and service of mineral geology and its metallogenic regularity in China” project of the China Geological Survey (grant no. DD20160346). In the process of drafting this

paper, Prof. Liu Suhong, Prof. Huang Miaofen of Beijing Normal University, and other experts gave me a lot of help. We have benefited from discussions of relevant contents with researcher Zhang Yujun of the Chinese Academy of Geological Sciences. We would like to acknowledge the people mentioned above for their constructive and thoughtful comments that helped us to improve the paper.

IntechOpen

IntechOpen

### **Author details**

Jiang Chen\*, Zhaoxia Mao, Yan Zhao, Chunpeng Zhang and Shan Jiang  
Shenyang Geological Center, CGS, Shenyang, Liaoning, China

\*Address all correspondence to: [chen07761@itc.nl](mailto:chen07761@itc.nl)

### **IntechOpen**

---

© 2019 The Author(s). Licensee IntechOpen. This chapter is distributed under the terms of the Creative Commons Attribution License (<http://creativecommons.org/licenses/by/3.0>), which permits unrestricted use, distribution, and reproduction in any medium, provided the original work is properly cited. 

## References

- [1] Bogoch R, Shirav M, Beyth M, Halicz L. Geochemistry of ephemeral stream sediments in the Precambrian mountainous arid terrain of southern Israel. *Journal of Geochemical Exploration*. 1993;**46**(3):349-364
- [2] Brantley SL, White AF. Approaches to modeling weathered regolith. *Reviews in Mineralogy and Geochemistry*. 2009;**70**(1):435-484
- [3] Cheng Q, Bonham-Carter G, Wang W, Zhang S, Li W, Qinglin X. A spatially weighted principal component analysis for multi-element geochemical data for mapping locations of felsic intrusions in the Gejiu mineral district of Yunnan, China. *Computers & Geosciences*. 2011;**37**(5):662-669
- [4] Hao LB, Lu JL, Li L, Mo GS, Yan GS, Shi YX, Zhao YY. Method of using regional geochemical data in geological mapping in shallow overburden areas. *Geology in China*. 2007;**4**:023 (in Chinese with English abstract)
- [5] Wang W, Zhao J, Cheng Q, Liu J. Tectonic-geochemical exploration modeling for characterizing geo-anomalies in southeastern Yunnan district, China. *Journal of Geochemical Exploration*. 2012;**122**:71-80
- [6] Zhao J, Wang W, Cheng Q. Application of geographically weighted regression to identify spatially non-stationary relationships between Fe mineralization and its controlling factors in eastern Tianshan, China. *Ore Geology Reviews*. 2014;**57**:628-638
- [7] Drury SA, Drury SA. *Image Interpretation in Geology*. London: Blackwell science; 2001. pp. 1-290
- [8] Gupta RP. *Remote Sensing Geology*. Springer Science & Business Media; 2013
- [9] Bedini E. Mapping lithology of the Sarfartoq carbonatite complex, southern West Greenland, using HyMap imaging spectrometer data. *Remote Sensing of Environment*. 2009;**113**(6):1208-1219
- [10] Berger BR, King TV, Morath LC, Phillips JD. Utility of high-altitude infrared spectral data in mineral exploration: Application to northern Patagonia mountains, Arizona. *Economic Geology*. 2003;**98**(5):1003-1018
- [11] Bierwirth P, Huston D, Blewett R. Hyperspectral mapping of mineral assemblages associated with gold mineralization in the Central Pilbara, Western Australia. *Economic Geology*. 2002;**97**(4):819-826
- [12] Kozak PK, Duke EF, Roselle GT. Mineral distribution in contact-metamorphosed siliceous dolomite at Ubehebe Peak, California, based on airborne imaging spectrometer data. *American Mineralogist*. 2004;**89**(5-6):701-713
- [13] Rockwell BW, Hofstra AH. Identification of quartz and carbonate minerals across northern Nevada using ASTER thermal infrared emissivity data—Implications for geologic mapping and mineral resource investigations in well-studied and frontier areas. *Geosphere*. 2008;**4**(1):218-246
- [14] Rowan LC, Mars JC. Lithologic mapping in the Mountain Pass, California area using advanced spaceborne thermal emission and reflection radiometer (ASTER) data. *Remote Sensing of Environment*. 2003;**84**(3):350-366
- [15] van Ruitenbeek FJ, Cudahy T, Hale M, van der Meer FD. Tracing fluid pathways in fossil hydrothermal systems

- with near-infrared spectroscopy. *Geology*. 2005;**33**(7):597-600
- [16] Windeler DS, Lyon RJP. Discrimination dolomitization of marble in the Ludwig skarn near Yerington, Nevada using high-resolution airborne infrared imagery. *Photogrammetric Engineering and Remote Sensing*. 1991;**57**(9):1171-1177
- [17] Chabrilat S, Pinet PC, Ceuleneer G, Johnson PE, Mustard JF. Ronda peridotite massif: Methodology for its geological mapping and lithological discrimination from airborne hyperspectral data. *International Journal of Remote Sensing*. 2000;**21**(12):2363-2388
- [18] Harris JR, Rogge D, Hitchcock R, Ijewliw O, Wright D. Mapping lithology in Canada's Arctic: Application of hyperspectral data using the minimum noise fraction transformation and matched filtering. *Canadian Journal of Earth Sciences*. 2005;**42**(12):2173-2193
- [19] Launeau P, Girardeau J, Sotin C, Tubia JM. Comparison between field measurements and airborne visible and infrared mapping spectrometry (AVIRIS and HyMap) of the Ronda peridotite massif (south-west Spain). *International Journal of Remote Sensing*. 2004;**25**(14):2773-2792
- [20] Rivard B, Zhang J, Feng J, Sanchez-Azofeifa GA. Remote predictive lithologic mapping in the Abitibi Greenstone Belt, Canada, using airborne hyperspectral imagery. *Canadian Journal of Remote Sensing*. 2009;**35**(sup1):S95-S105
- [21] Roy R, Launeau P, Carrere V, Pinet P, Ceuleneer G, Clenet H, et al. Geological mapping strategy using visible near-infrared–shortwave infrared hyperspectral remote sensing: Application to the Oman ophiolite (Sumail Massif). *Geochemistry, Geophysics, Geosystems*. 2009;**10**(2):1-23
- [22] Van der Meer FD, Van der Werff HM, van Ruitenbeek FJ, Hecker CA, Bakker WH, Noomen MF, et al. Multi- and hyperspectral geologic remote sensing: A review. *International Journal of Applied Earth Observation and Geoinformation*. 2012;**14**(1):112-128
- [23] Björklund A, Gustavsson N. Visualization of geochemical data on maps: New options. *Journal of Geochemical Exploration*. 1987;**29**(1):89-103
- [24] Gustavsson N, Lampio E, Tarvainen T. Visualization of geochemical data on maps at the Geological Survey of Finland. *Journal of Geochemical Exploration*. 1997;**59**(3):197-207
- [25] She HQ, Li HH, Li JW, Zhao SB, Tan G, Zhang DQ, et al. The metallogenetical characteristics and prospecting direction of the copper-lead-zinc polymetal deposits in the northern-central Daxing'anling Mountain, Inner Mongolia. *Acta Geologica Sinica*. 2009;**83**(10):1456-1472 (in Chinese with English abstract)
- [26] Miao L, Zhang F, Fan WM, Liu D. Phanerozoic evolution of the Inner Mongolia–Daxinganling orogenic belt in North China: Constraints from geochronology of ophiolites and associated formations. Geological Society, London, Special Publications. 2007;**280**(1):223-237
- [27] Zhang X, Zhang H, Tang Y, Wilde SA, Hu Z. Geochemistry of Permian bimodal volcanic rocks from central Inner Mongolia, North China: Implication for tectonic setting and Phanerozoic continental growth in Central Asian Orogenic Belt. *Chemical Geology*. 2008;**249**(3):262-281
- [28] Zhang L, Gao B, Li W, Chen Z, Sakyi PA, Jin X. Early Mesozoic

tectono-magmatic activity and mineralization in Northeast China: Evidence from Re–Os to U–Pb studies of the Taipingchuan porphyry Cu–Mo deposit in the Derbugan metallogenic belt. *International Geology Review*. 2014;**56**(15):1837-1851

[29] Xuejing X, Huanzhen S, Tianxiang R. Regional geochemistry-national reconnaissance project in China. *Journal of Geochemical Exploration*. 1989;**33**(1):1-9

[30] Cai YZ, Feng WH. A review of 1:200 000 regional geochemical exploration in the forest-swamp area of eastern inner Mongolia. *Geophysical & Geochemical Exploration*. 2003;**27**(6):423-424

[31] Wang HF, Ye ZC. The application of new 1:200 000 regional geochemical methods to Wuchagou sheet in Inner Mongolian forest-swamp area. *Geophysical & Geochemical Exploration*. 2003;**27**(6):435-437

[32] Akima H. A method of bivariate interpolation and smooth surface fitting for irregularly distributed data points. *ACM Transactions on Mathematical Software (TOMS)*. 1978;**4**(2):148-159

[33] Hecker C, Van der Meijde M, van der Werff H, Van der Meer FD. Assessing the influence of reference spectra on synthetic SAM classification results. *IEEE Transactions on Geoscience and Remote Sensing*. 2008;**46**(12):4162-4172

[34] Kruse FA, Lefkoff AB, Boardman JW, Heidebrecht KB, Shapiro AT, Barloon PJ, et al. The spectral image processing system (SIPS)—Interactive visualization and analysis of imaging spectrometer data. *Remote Sensing of Environment*. 1993;**44**(2):145-163

[35] Webb JS. Regional geochemical reconnaissance in the Namwala Concession area, Zambia (No. 47). 1964